Electromagnetic transition strengths between high spin states in ^{79}Sr and ^{80}Sr

J. Heese, K. P. Lieb, S. Ulbig, and B. Wörmann
II. Physikalisches Institut, Universität Göttingen, D-3400 Göttingen, Federal Republic of Germany

J. Billowes, A. A. Chishti, W. Gelletly,* C. J. Lister,† and B. J. Varley
Schuster Laboratory, University of Manchester, Manchester M13 9 PL, United Kingdom
(Received 2 May 1989)

High spin states in ^{79}Sr were populated via the reaction ^{58}Ni(^{24}Mg,2pn) at 80 and 85 MeV beam energy. Twelve lifetimes in the range from 0.5 to 150 ps and four lifetime limits were measured with Doppler-shift methods. By comparing lifetimes in ^{79,80,82}Sr obtained with the recoil distance and Doppler-shift attenuation methods, the appropriate electronic stopping power of Sr ions recoiling in Ta was determined. In addition, lifetimes of yrast states in ^{80}Sr and ^{79}Rb were determined in the concurrent reactions ^{58}Ni(^{24}Mg,2p) and ^{58}Ni(^{24}Mg,3p). The $\Delta I=2$ $E2$ transition strengths and the $E2/M1$ mixing ratios of the $\Delta I=1$ transitions in ^{79}Sr confirm the picture of extremely prolate deformed rotational bands ($\beta_2\approx 0.42$), based on the $[301]\frac{3}{2}^-$ and $[422]\frac{5}{2}^+$ Nilsson orbitals. A reduction in $B(E2)$ values is observed at the onset of (3qp) alignment. The band structure of ^{79}Sr is discussed in terms of the cranked shell and the Woods-Saxon cranking model with pairing.

I. INTRODUCTION

Detailed in-beam studies of the light strontium isotopes by means of heavy-ion fusion evaporation reactions have revealed evidence for complex band structures.[1–4] Davie and collaborators[2] recently investigated ^{80}Sr and identified stretched $E2$ transitions for three bands, in addition to the ground band which they extended up to spin 26$\hbar$. These bands were found to have $E2$ strengths of 80–180 single-particle units and moments of inertia steadily increasing with spin. The bands observed in the heavier Sr isotopes ^{82,84}Sr are less deformed.[3,4] On the basis of shell-model arguments and magnetic-moment measurements,[5,6] some of the s bands have been assigned to two-quasiparticle $g_{9/2}$ proton or neutron aligned configurations.

The odd-A nuclei in this mass region are of interest because they reveal the details of the interplay between the single-particle states occupied by the odd nucleus and the collective "cores." Dramatic changes in shape have been observed which depend on the density of the single-particle states and the variation of their energies with deformation. A very good example is the core-polarization effect in ^{81}Sr ($N=43$) in the $[431]\frac{1}{2}^+$ Nilsson orbital which intrudes from the $d_{5/2}$ shell. Moore *et al.*[7] found that the rotational band based on this orbital has a transitional quadrupole moment of $|Q_t|=3.5(6)$ b, whereas the $g_{9/2}$ band in ^{81}Sr only shows $|Q_t|=1.9(4)$ b. The $[431]\frac{3}{2}^+$ bandhead in ^{81}Sr has a small excitation energy of 120 keV and its deformation is quite similar to that expected in ^{79}Sr. Since the Fermi energies for $N=43$ and 41 at deformation $\beta_2\approx 0.4$ should be comparable,[8] the $[431]\frac{1}{2}^+$ orbital is also expected to play a role in the structure of ^{79}Sr.

In general, an unpaired $g_{9/2}$ proton in a *low*-Ω orbit induces an increase in deformation and a nearly rigid (often triaxial) rotation up to high rotational frequencies. Additional $g_{9/2}$ quasiparticle proton alignments are difficult to observe, probably because they are blocked by a $g_{9/2}$ proton pair. In contrast, the situation in the odd-neutron nuclei is different, since the low-Ω Nilsson orbits are filled and the full rotational alignment of the $g_{9/2}$ neutron(s) cannot take place. This has been convincingly demonstrated by Wörmann *et al.*[9] in a comparison of the $E2$ transition strengths in the $N=41$ isotone ^{77}Kr with those in ^{76}Kr. Furthermore, the $g_{9/2}$ (2qp) proton alignment combined with partial $g_{9/2}$ neutron alignment leads to a mixed coupling scheme for the (3qp) yrast bands as pointed out by Funke *et al.*[10] in the case of ^{81}Kr.

The positive- and negative-parity yrast sequences in ^{79}Sr have recently been established by Chishti *et al.*[11] up to probable spins $\frac{37}{2}^+$ and $\frac{33}{2}^-$, and fairly regular band structures were found as shown in Fig. 1. The most obvious irregularity is an upbend in the positive-parity band at spin $\frac{25}{2}^+$. Indeed, the $\frac{29}{2}^+\rightarrow\frac{25}{2}^+$ and the $\frac{25}{2}^+\rightarrow\frac{21}{2}^+$ transitions have exactly the same γ-ray energy of 1175 keV. The present lifetime measurements, made with the recoil distance and Doppler-shift attenuation (DSA) techniques, were intended to determine the collectivity and structure of the (1qp) bands and to shed light on the alignment effects occurring at the onset of the (3qp) bands.

II. EXPERIMENTAL PROCEDURE

The reaction ^{58}Ni(^{24}Mg,2pn)^{79}Sr was studied with a beam of 10–20 nA of ^{24}Mg^{7+} ions supplied by the Oxford folded tandem accelerator. The beam energies chosen, 80 MeV in the recoil distance and 85 MeV in the DSA experiments, ensured the optimum population of the states of interest.

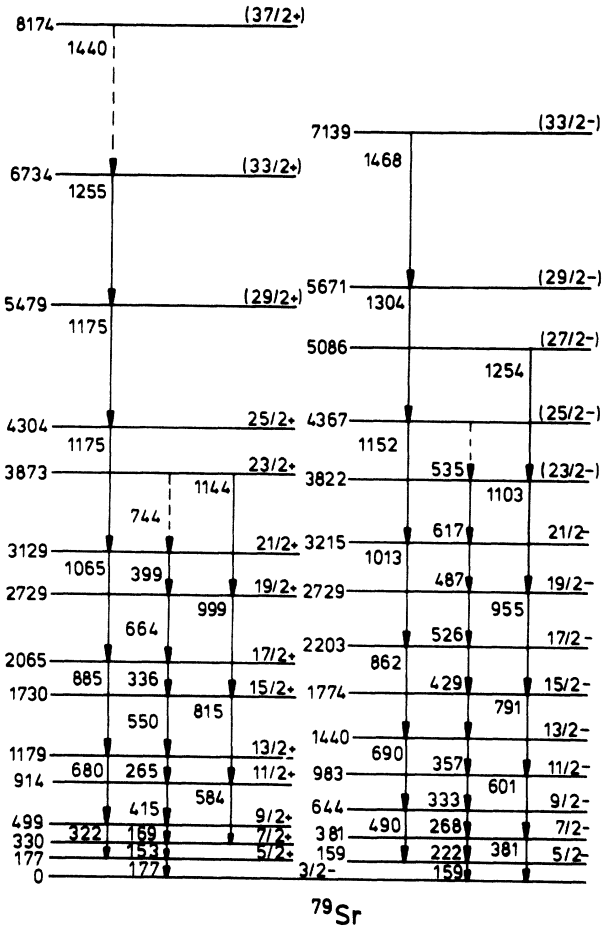

FIG. 1. The decay scheme of high spin states in ^{79}Sr (Ref. 11).

A. The recoil distance experiment

The design of the plunger apparatus has been described previously.[12] The beam enters the target chamber through a 3-mm diameter lead collimator and hits the target, which consists of a thin self-supporting, stretched foil of ≈ 0.7-mg/cm^2 thickness enriched to 99.98% in ^{58}Ni. The recoil nuclei travel at an average velocity of $v/c = 2.05(2)\%$ along a variable flight path D before they are stopped in a 20-μm thick stretched Ta foil. The flight distance is set by a micrometer screw to a precision of ± 1 μm and is continuously monitored by means of a magnetic transducer (± 0.1 μm) and the digitized capacity of the target-stopper system. The distance calibration was carried out with the beam hitting the target to ensure that additional thermal effects were minimized. A further check was available because it was possible to measure the known lifetimes of states in ^{76}Kr, ^{80}Sr, and ^{79}Rb (Refs. 1, 2, 9, 13) which are produced in the $\alpha 2p$, $2p$, and $3p$ channels of the ^{24}Mg+^{58}Ni reaction. This comparison is shown in Table I. The agreement with the previously measured lifetimes over a range from 1 to 50 ps is excellent. The present experiment has also provided more precise lifetime values for the 2^+ and 4^+ yrast states in ^{80}Sr than those obtained previously.[1,2]

The γ radiation was observed at 0° to the beam in a Ge detector of 25% relative efficiency at a 1.33-MeV photon energy with a bismuthe germanate (BGO) Compton suppression shield. A second Ge detector, without Compton suppression, was placed at 142° to the beam. This allowed us to locate the Doppler-shifted peaks in parts of the spectrum where they did not overlap with other lines, at least at one of the two detector angles. The spectra in both detectors were cleaned further with respect to the strong Coulomb excitation lines in ^{24}Mg, ^{58}Ni, and ^{181}Ta by requiring coincidences with γ rays observed in either a 12.5-cm diameter, 12.5-cm long NaI($T1$) detector or an eight-segment BGO detector of similar size. Since the γ-ray multiplicity of the evaporation residues is much higher than the γ-ray multiplicity following Coulomb excitation or β decays, the latter are suppressed in the gated spectra. This simple γ-ray filter, together with Compton suppression, allowed us to identify small flight- or stop-peak intensities. Thus, we were able to scan a larger dynamic range in the decay functions. Figure 2 shows parts of the 0° spectra taken at $D = 2$ and 750 μm.

Spectra were recorded at 22 distances (chosen in random order) between electrical contact (≤ 2 μm) and 5

TABLE I. Comparison of lifetimes from the present recoil distance analysis and previous work.

Nucleus	Transition		Lifetime τ (ps) Present work	Previous work	Reference
^{80}Sr	386	$2^+ \rightarrow 0^+$	49.4(18)	53(4)	1
	595	$4^+ \rightarrow 2^+$	4.2(2)	4.8(7)	1
^{79}Rb	547	$\frac{11}{2}^+ \rightarrow \frac{7}{2}^+$	8.5(2)	8.2(4)	13
	501	$\frac{13}{2}^+ \rightarrow \frac{9}{2}^+$	11.4(10)	11.9(6)	13
	810	$\frac{15}{2}^+ \rightarrow \frac{11}{2}^+$	1.2(2)[a]	1.3[a]	13
^{76}Kr	424	$2^+ \rightarrow 0^+$	37.7(30)	35.6(10)	9

[a]Effective value not corrected for feeding.

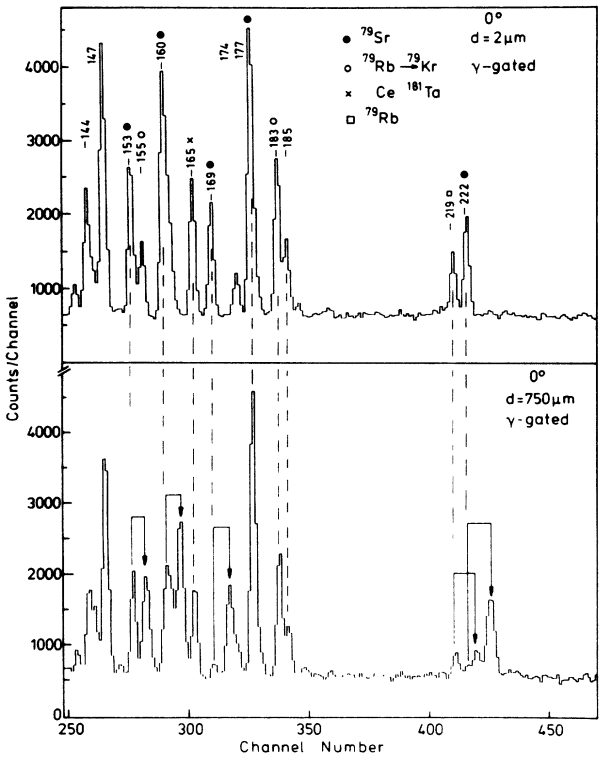

FIG. 2. Portions of the Compton suppressed 0° spectra taken at recoil distance $D=2$ μm (electrical contact between target and stopper) and $D=750$ μm.

mm; this covers the time range up to a few ns. The stopped- and flight-peak intensities in both detectors were determined in the γ-ray singles and gated spectra and were normalized to the intensity of the 301-keV Coulomb excitation line in ^{181}Ta which is proportional to the accumulated beam charge. Several decay functions are plotted in Fig. 3. The fits shown were obtained with the program CHRONOS (Ref. 14) which considers up to five feeding components (see below). Corrections to the decay functions due to the finite spread in recoil velocity, the finite detector size, and the time-dependent hyperfine deorientation were neglected for reasons discussed previously.[12,15] Feeding-time effects will be discussed in Sec. III A.

B. The Doppler-shift attenuation experiment

The lifetimes of the states with spins $>17/2\hbar$ are too short to be measured by means of the recoil distance technique but are accessible to the DSA method. Such a measurement was carried out at a 85-meV beam energy using a 380-μg/cm^2 ^{58}Ni layer evaporated onto a 100-μm Ta backing and placed at 45° to the beam. The beam intensity has 20 nA and the γ-ray spectra were accumulated for 78 h.

While neutron evaporation from the ^{82}Zr compound nucleus and along the evaporation chains is a fairly rare process, the ^{76}Kr+α2p, ^{79}Rb+3p, and ^{78}Kr+4p channels are most strongly populated. Therefore, the common method of measuring Doppler broadened line shapes in the $\gamma\gamma$ coincidence mode, and gating on the respective

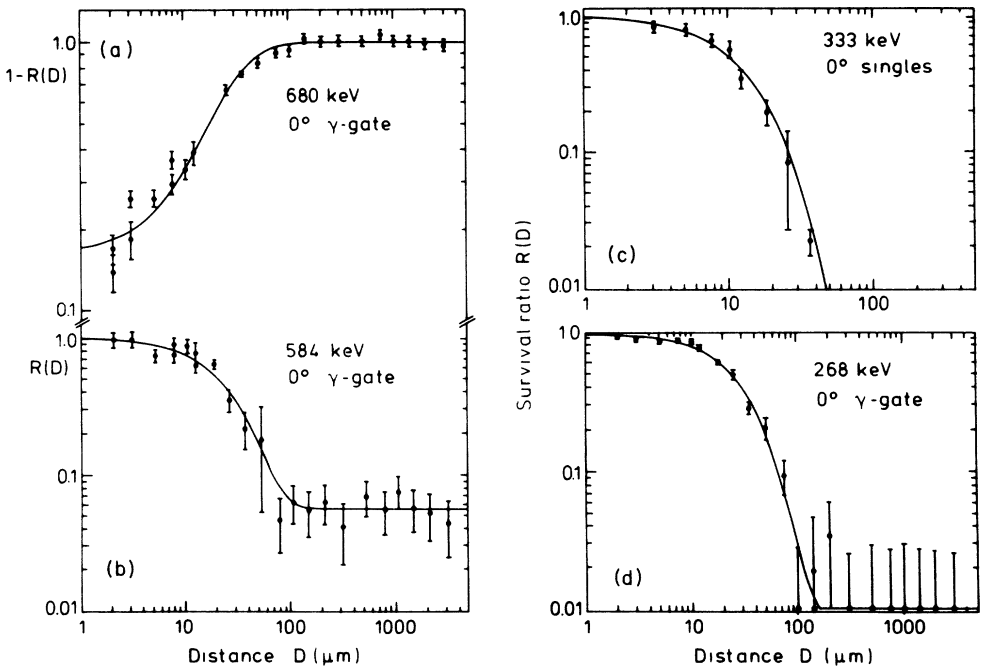

FIG. 3. Survival ratios for some yrast transitions in ^{79}Sr.

in-band transitions was not feasible. We thus measured line shapes in ^{79}Sr by gating the Compton suppressed Ge detector at 0° with the signals from four conical NE213 neutron detectors which covered some 20% of the total solid angle. By gating on the evaporated neutrons, we not only discriminated against the strong charged particle evaporation channels, but also against Coulomb excitation and β-decay cascades. A sample spectrum is displayed in Fig. 4; it predominantly contains lines from the ^{79}Sr+2*pn* channel and also, with lower intensity, from the ^{78}Rb+3*pn* channel.[16] Since there are bands with similar deformations in both nuclei, the ^{79}Sr and ^{78}Rb γ rays have similar energies, and the probability that the ^{79}Sr lines are contaminated is quite high. In the more favorable cases, the intensity of the contaminating line was small enough to cause uncertainties in the lifetime analysis of only about 10%, i.e., in the case of the 1065-keV $\frac{21}{2}^+ \rightarrow \frac{17}{2}^+$ transition in ^{79}Sr which is contaminated by a 1080-keV ^{78}Rb line.[16] In other cases the number of overlapping lines prevented reliable DSA lineshape analyses, e.g., in the case of the 1013-keV $\frac{21}{2}^- \rightarrow \frac{17}{2}^-$ line which is contaminated by the 999-keV $\frac{19}{2}^+ \rightarrow \frac{15}{2}^+$ transition in ^{79}Sr, and the 1013- and 1020-keV lines in ^{78}Rb. For similar reasons the 955-keV ($\frac{19}{2}^- \rightarrow \frac{15}{2}^-$), 1253-keV ($\frac{33}{2}^+ \rightarrow \frac{29}{2}^+$), and 1255-keV ($\frac{27}{2}^- \rightarrow \frac{23}{2}^-$) multiplets could not be analyzed. Furthermore, no DSA analysis of the 1175-keV $\frac{29}{2}^+ \rightarrow \frac{25}{2}^+$ and $\frac{25}{2}^+ \rightarrow \frac{21}{2}^+$ doublet was possible.

III. ANALYSIS OF THE LIFETIME DATA AND RESULTS

It is well known that the analysis of recoil distance decay functions and Doppler broadened lines shapes following heavy-ion fusion reactions is sensitive to the feeding intensities and times, including (continuum) side feeding times. In addition, the process of the slowing down of the excited nuclei in the stopping material strongly affects the lifetimes deduced from the DSA analysis. For these reasons we discuss in this section the assumptions and tests made concerning these parameters. The Doppler broadened line shapes were fitted with the code GNOMON (Ref. 17) as described in several recent papers.[18,19]

A. Feeding pattern

Great care was taken to use the correct feeding intensities in the analysis. For this reason, singles spectra of good statistics were accumulated at 55° to the beam where the angular distribution effects are at a minimum. In order to avoid systematic errors due to overlapping lines in the 55° γ-ray singles spectra, the intensities of some ^{79}Sr lines were also determined in the 0° neutron gated spectra where those lines were clearly separated. In particular, the relative intensities of the Doppler broadened $\Delta I=2$ transitions were obtained at 0° in the neutron gated spectra. Their relative intensities were then corrected for angular distribution effects using the

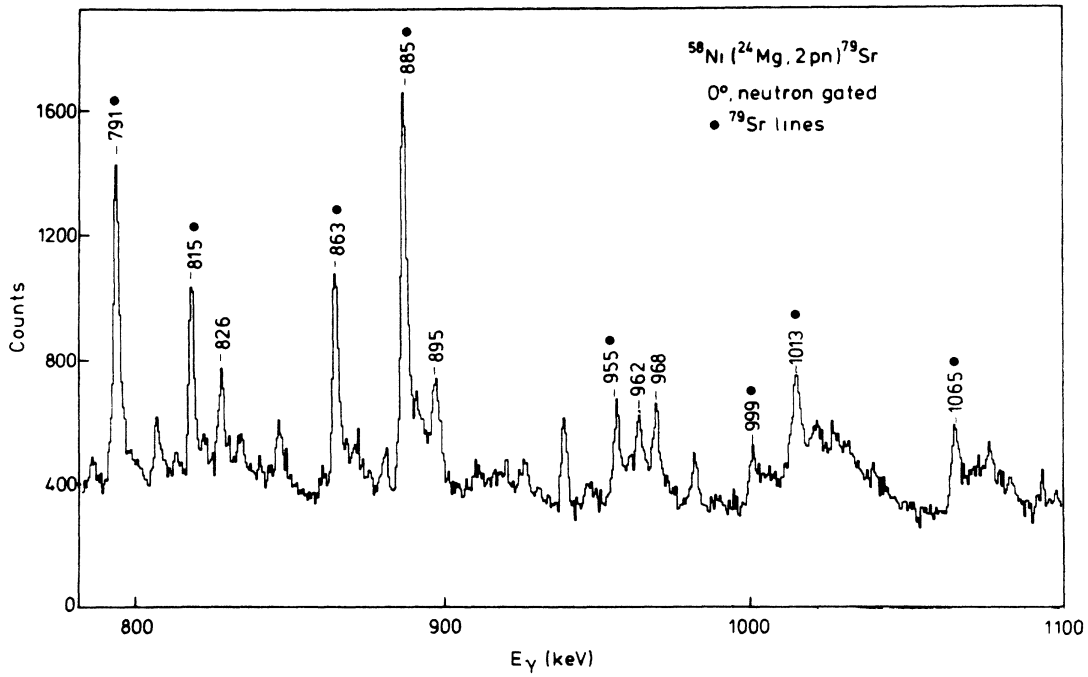

FIG. 4. Portion of the Compton suppressed and neutron gated 0° spectrum. The energies inserted refer to transitions in ^{79}Sr. For details see text.

known a_2 and a_4 angular distribution coefficients.[1,20]

The second source of systematic errors, the side feeding time τ_F, has been investigated in several previous studies.[2,18,21–24] It was found that τ_F can be as large as, or even exceed the lifetime of, the level it is feeding. In the present experiment the side average feeding times were taken into account by fitting the DSA line shapes for fixed values of τ_F in the range from zero to 1 ps. In most cases the reduced goodness-of-fit parameter χ_r^2 only gave a lower limit for τ_f. An upper limit for τ_f could not be determined from the χ_r^2 arguments since, for long feeding times of $\tau_f \geq 0.3$ ps, good fits could always be achieved with correspondingly shorter level lifetimes.

For the $\frac{17}{2}^+$ level, this procedure gave a lower limit of $\tau_f \geq 0.15$ ps, while the χ_r^2 minimum was located at $\tau_f = 0.25$ ps. It was assumed that the side feeding time for this level does not exceed 0.5 ps. With $\tau_f = 0.25(^{25}_{10})$ ps the lifetime of the $\frac{17}{2}^+$ state was determined to be

$$\tau(\tfrac{17}{2}^+) = 0.69(^{7}_{10})\ \text{ps} .$$

The side feeding times for the other levels were estimated by assuming that the feeding times for a given spin are equal in the positive- and negative-parity bands (on the basis of the conformity of the level energies in both bands) and increase with decreasing spin by $\Delta\tau_f/\Delta I \approx 0.1$ ps/$\hbar$. In addition, the feeding times in ^{79}Sr have been stimulated with the most recent version of our Monte Carlo code GAMMAPACE, which gives a most convincing agreement for measured and simulated feeding times in the reaction ^{54}Fe(^{32}S,3p)^{83}Y at a beam energy of 103 MeV.[18] Details of the model are also discussed in Refs. 18 and 21. The ^{79}Sr simulation was done assuming that the average collective $E2$ strengths of the 125 Weiskopf unit (W.u.) are exponentially decreasing within a 1-MeV $1/e$ wide band above the yrast line. The calculated feeding times $\tau_f(\frac{21}{2}) = 0.11$ ps, $\tau_f(\frac{17}{2}) = 0.19$ ps, $\tau_f(\frac{13}{2}) = 0.31$ ps, and $\tau_f(\frac{9}{2}) = 0.56$ ps are in good agreement with the assumed range of feeding times included in Table II. The level lifetimes were again obtained by calculating the correlation between τ and τ_f. The errors in the level lifetimes correspond to the feeding-time range. The effective lifetimes of the $\frac{25}{2}^+$ and $\frac{21}{2}^-$ states were determined from the line-shape fits to the $\frac{21}{2}^+ \rightarrow \frac{17}{2}^+$ and $\frac{17}{2}^- \rightarrow \frac{13}{2}^-$ transitions where the effective lifetimes were fitted as additional free parameters.

In the recoil distance analysis side feeding times were only taken into account for lifetimes below 3 ps. They were assumed to be equal in the recoil distance (RD) and DSA experiments. This is supported by the good agreement between RD and DSA lifetime values for the $\frac{15}{2}^-$ and $\frac{17}{2}^-$ states.

B. Stopping power function

In ^{79}Sr we were able to measure the lifetimes of the $\frac{15}{2}^-$ and $\frac{13}{2}^-$ states with both the RD and DSA methods. The analysis of the recoil distance data does not depend on the stopping power as long as the level lifetime exceeds the slowing down time in the stopper foil. A comparison of lifetimes determined with both methods then allows one to select the appropriate stopping power function in the DSA analysis and thus reduce the systematic errors in the lifetimes. In order to investigate this point in more detail, we also considered excited states in the evaporation residues ^{80,82}Sr, the lifetimes of which were again accessible to both methods. These nuclei were populated in the reactions ^{54}Fe(^{32}S,$\alpha 2p$)^{80}Sr and ^{54}Fe(^{32}S,4p)^{82}Sr at beam energies of 103 and 107 MeV. This experiment is a by-product of our recent detailed lifetime studies in ^{83}Y and ^{83}Zr, performed with the University of Cologne tandem accelerator: details can be found in Refs. (18 and 19). In ^{80}Sr, lifetimes of the 2700-keV 8^+ and 1763-keV 6^+ yrast states were determined by both methods. For the 3243-keV 8^+ and 2230-keV 6^+ yrast states in ^{82}Sr only the DSA method was applied, but here precise RD results are available from the work of Dewald *et al.*[25]

To fit the Doppler broadened line shapes we used the parametrization of Kalbitzer and Oetzmann[26] for the nuclear component of the stopping power function and treated the angular straggling of the ions according to Blaugrund.[27] For the electronic component of the stopping power function, we considered the parametrizations of Northcliffe and Schilling[28] labeled NS, and of Ziegler,

TABLE II. Lifetimes and $E2$ transition strengths in the ^{80}Sr ground band from present and previous work.

State	I^π	Mean lifetime τ (ps) Present	Previous	Adopted	$B(E2)$ (e^2fm^4)	$\lvert Q_t \rvert$ (b)
386	2^+	49.4(18)	53(4)[a] 63(9)[b]	52(2)	1840(70)	3.04(6)
981	4^+	4.2(2)	4.8(7)[c]	4.3(2)	2550(120)	2.99(7)
1764	6^+	0.82(8)	1.8(11)[c]	0.96(14)	2890($^{490}_{360}$)	3.04($^{25}_{20}$)
2701	8^+	0.47(6)	0.32(13)[c]	0.42(6)	2700($^{440}_{340}$)	2.87($^{23}_{19}$)
3766	10^+	0.49(2)[d]	0.25(11)[c]	0.25(11)	2390($^{1870}_{730}$)	2.66($^{90}_{44}$)

[a]Reference 1.
[b]Reference 41.
[c]Reference 2.
[d]Effective lifetime not corrected for feeding.

TABLE III. Comparison of lifetimes in ^{79,80,82}Sr obtained from recoil distance and DSA measurements.

Nucleus	I^π	τ_{RD} (ps)	τ_{DSA} (ps)		
			NS	NS*0.7	ZBL
^{79}Sr	$\frac{15}{2}^-$	1.4(2)[a]	1.25(10)[a]	1.49(10)[a]	1.41(10)[a]
	$\frac{13}{2}^-$	1.3(3)	1.05(9)	1.44(12)	1.28(10)
^{80}Sr	10^+		0.47(2)[a]	0.59(3)[a]	0.49(2)[a]
	8^+	1.1(2)[a]	0.83(8)[a]	1.02(10)[a]	0.91(9)[a]
		0.54(10)[b]	0.40(1)[b]		0.45(1)[b]
		0.43(8)[c]		0.48(10)[c]	
	6^+	0.80(9)	0.70(7)	0.89(8)	0.84(8)
^{82}Sr	8^+		0.83(8)[a]	1.02(10)[a]	0.91(9)[a]
	6^+	1.3(2)[d]	0.87(9)	1.05(11)	0.92(9)

[c]Effective lifetime not corrected for feeding.
[b]$\tau_{eff}(10^+)=0.47$ ps.
[c]$\tau_{eff}(10^+)=0.59$ ps.
[d]Taken from Reference 3.

Biersack, and Littmark[29] labeled ZBL. Since the DSA lifetime values with the NS stopping powers (see Table III) turned out to be systematically shorter than the RD lifetime values, we had to multiply the NS stopping power by a constant factor 0.7 in order to achieve agreement with the RD results. This set of data is labeled "NS*0.7" in Table III. The lifetimes given there have been calculated with a fixed side feeding time $\tau_f=0.2$ ps in order to reduce the errors in the comparison of τ_{RD} and τ_{DSA}.

DSA line-shape fits and RD decay functions for some of the transitions in ^{79,80}Sr are presented in Figs. 5 and 6. For the 783-keV $6^+\rightarrow 4^+$ transition in ^{80}Sr, a long component in the recoil distance decay function was observed with a lifetime of about 30 ps. This component arises from the feeding from (7*) states into the 6^+ state, but it was neglected in the analysis due to its weak feeding intensity of less than 10% of the total feeding into the 6^+ state. Since no recoil distance lifetimes in ^{82}Sr were obtained in the present experiment, a comparison was made

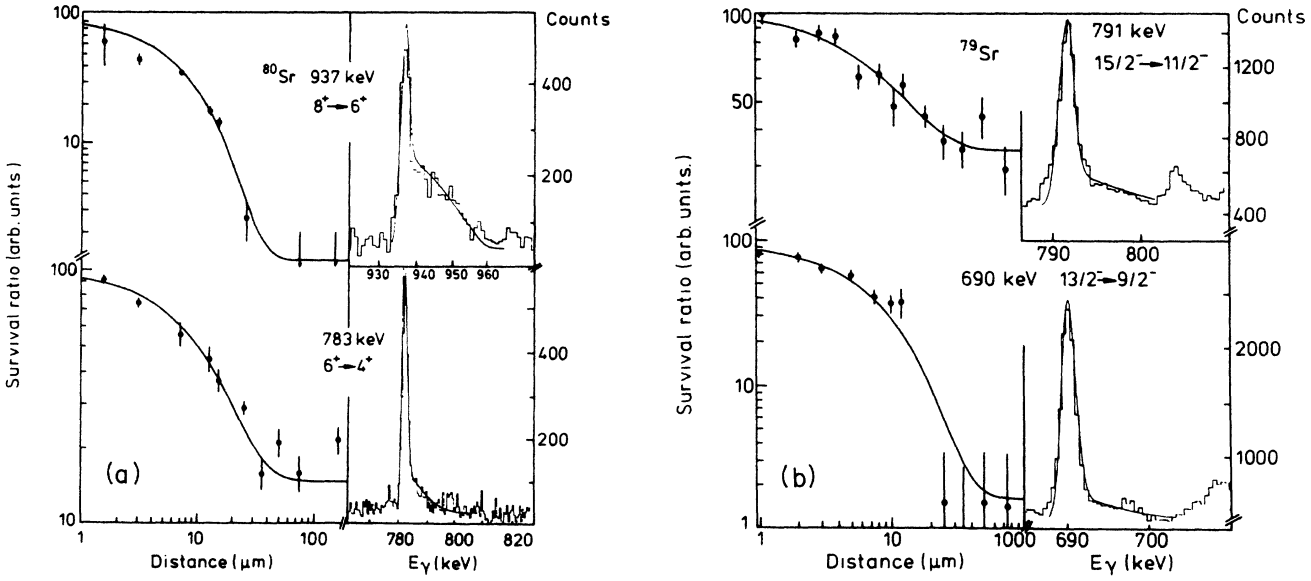

FIG. 5. Survival ratios and Doppler broadened line shapes for (a) the $8^+\rightarrow 6^+$ and $6^+\rightarrow 4^+$ transitions in ^{80}Sr and (b) the $\frac{15}{2}^-\rightarrow\frac{11}{2}^-$ and $\frac{13}{2}^-\rightarrow\frac{9}{2}^-$ transitions in ^{79}Sr.

with previous work.[25] The RD value of the 6^+ state is slightly larger than the DSA value of Ref. 25, probably due to the neglected side feeding time in the latter RD analysis. Since the ZBL parametrization, which is based on the most recent and complete evaluation of stopping power data,[29] gave satisfactory agreement with the RD lifetimes, it was adopted in all of the other DSA analyses in ^{79}Sr.

C. Lifetime results

The measured lifetimes in ^{79}Sr are summarized in Table IV, together with the measured intensities and

TABLE IV. Level energies, transition energies, intensities, branching ratios, and lifetimes in ^{79}Sr.

E_x (keV)	E_γ (keV)	I_i^π	I_f^π	I_γ (%)	b (%)	τ (ps)
177.4	177.4	$\frac{5}{2}^+$	$\frac{3}{2}^-$	118.1(36)	100	20(1) ns[a]
329.9	152.5	$\frac{7}{2}^+$	$\frac{5}{2}^+$	98.4(30)	100	154(9)
499.2	169.0	$\frac{9}{2}^+$	$\frac{7}{2}^+$	51.9(21)	81.1(12)	44(5)
	322.1		$\frac{5}{2}^+$	12.1(5)	18.9(12)	
914.3	415.1	$\frac{11}{2}^+$	$\frac{9}{2}^+$		60(2)[a]	2.6(3)
	584.3		$\frac{7}{2}^+$	14.1(10)	40(2)[a]	$\tau_f=0.5(2)$
1179.3	264.9	$\frac{13}{2}^+$	$\frac{11}{2}^+$	7.5(4)	21.1(20)	1.7(3)
	680.1		$\frac{9}{2}^+$	27.8(14)	78.9(20)	$\tau_f=0.4(2)$
1729.5	550.2	$\frac{15}{2}^+$	$\frac{13}{2}^+$	5.4(5)	31.5(55)	<1.0
	815.2		$\frac{11}{2}^+$	12.0(20)	68.5(55)	
2065.0	335.6	$\frac{17}{2}^+$	$\frac{15}{2}^+$	3.0(4)	12.3(21)	$0.69(^{7}_{10})$
	884.5		$\frac{13}{2}^+$	21.4(11)	87.7(21)	$\tau_f=0.25(^{25}_{10})$
2729.1	664.4	$\frac{19}{2}^+$	$\frac{17}{2}^+$	2.2(3)		
	999.3		$\frac{15}{2}^+$			
3129.3	399.3	$\frac{21}{2}^+$	$\frac{19}{2}^+$	3.6(5)	18.3(32)	0.52(10)
	1065.2		$\frac{17}{2}^+$	16.1(13)	81.7(32)	$\tau_f=0.15(^{20}_{10})$
4304	1175	$\frac{25}{2}^+$	$\frac{21}{2}^+$			<0.30[d]
159.5	159.5	$\frac{5}{2}^-$	$\frac{3}{2}^-$	100.0(20)	100	70(9)
381.3	221.7	$\frac{7}{2}^-$	$\frac{5}{2}^-$	54.4(17)	84.9(9)	18(3)
	381.3		$\frac{3}{2}^-$	9.7(4)	15.1(9)	
649.5	268.1	$\frac{9}{2}^-$	$\frac{7}{2}^-$	26.0(13)	60.2(24)	4.3(7)
	490.1		$\frac{5}{2}^-$	17.2(9)	39.8(24)	
982.7	333.2	$\frac{11}{2}^-$	$\frac{9}{2}^-$	13.6(12)	48.0(54)	1.5(2)
	601.4		$\frac{7}{2}^-$	14.8(19)	52.0(54)	$\tau_f=0.5(2)$
1339.8	357.0	$\frac{13}{2}^-$	$\frac{11}{2}^-$	9.0(7)	32.0(28)	1.25(20)[b]
	690.3		$\frac{9}{2}^-$	19.2(10)	68.0(28)	$\tau_f=0.4(2)$
1774.0	434.6	$\frac{15}{2}^-$	$\frac{13}{2}^-$	4.3(5)	22.4(34)	1.4(1)[c]
	791.0		$\frac{11}{2}^-$	15.0(12)	77.6(34)	
2202.5	428.5	$\frac{17}{2}^-$	$\frac{15}{2}^-$	3.6(5)	23.4(43)	0.90(15)
	862.7		$\frac{13}{2}^-$	11.8(12)	76.6(43)	$\tau_f=0.25(^{25}_{10})$
2729.0	526.2	$\frac{19}{2}^-$	$\frac{17}{2}^-$	1.0(3)		
	955.4		$\frac{15}{2}^-$			
3215	487	$\frac{21}{2}^-$	$\frac{19}{2}^-$			<0.6[d]
	1013		$\frac{17}{2}^-$			

[a]Reference 20.
[b]Average value of $\tau_{RD}=1.3(3)$ ps and $\tau_{DSA}=1.2(3)$ ps.
[c]Effective lifetime, average of $\tau_{RD}=1.4(2)$ ps and $\tau_{DSA}=1.4(1)$ ps.
[d]Effective lifetime not corrected for feeding.

branching ratios. The experimental errors of the DSA lifetimes only contain statistical errors and uncertainties due to the range of τ_f. The deduced electromagnetic transition strengths will be discussed below.

A summary of lifetimes of the four lowest transitions in ^{80}Sr obtained in the present and previous work[1,2] is given in Table II. The effective lifetimes of the 6^+ and 8^+ state in ^{80}Sr were measured by the RD method in the ^{58}Ni(^{24}Mg,$2p$)^{80}Sr and ^{54}Fe(^{32}S,$\alpha 2p$)^{80}Sr reactions. The resulting values $\tau_{\text{eff}}(8^+)=1.1(2)$ and $\tau_{\text{eff}}(6^+)=1.6(2)$ ps do not seem to be caused by long feeding times in the ps range as reported by Davie *et al.*[2] In the present work, the influence of the side feeding times was treated similarly as in ^{79}Sr, i.e., τ_f was neglected for the long-lived 2^+ and 4^+ states, but was assumed to be $\tau_f=0.2(\frac{3}{2})$ ps in the analysis of the 6^+ and 8^+ states. The $B(E2)$ values corresponding to the adopted lifetimes given an average transitional quadrupole moment of $|Q_t|=3.00(6)$ b.

IV. DISCUSSION

A. The 1qp bandheads

A recent measurement of the ground-state spin in ^{79}Sr by laser spectroscopy[30] has confirmed the $I^\pi=\frac{3}{2}^-$ spin-parity assignment made by Lister *et al.*[1] According to the single-particle scheme calculated with a Woods-Saxon potential,[8] the 41st neutron occupies the $[301]\frac{3}{2}^-$ orbit, at large *prolate* deformation. This orbit is also accessible, however, at large *oblate* deformation and the measured spin does not allow us to determine the sign of the deformation. On the other hand, the $E2/M1$ mixing ratios $\delta(E2/M1)$ of the $\Delta I=1$ in-band transitions depend on this sign and furthermore distinguish between different Nilsson orbits. We therefore compared the experimental $E2/M1$ mixing ratios with those evaluated with the Nilsson model in the limit of axial symmetry ($\gamma=0°$ or $-60°$) and the well-defined projection quantum number Ω.[31] δ is given by

$$\delta(E2/M1)=[0.933E_\gamma(\text{MeV})/(I_i^2-1)^{1/2}] \times[1+\delta_{\Omega,1/2}(-)^{I+1/2}b]Q_t/(g_\Omega-g_R)\,. \quad (1)$$

Here, I_i is the initial spin and E_γ is the transition energy, Q_t is the (transitional) quadrupole moment, $g_\Omega-g_R$ is the difference between the single particle and collective g factors, and b is a term related to the decoupling parameter in $\Omega=\frac{1}{2}$ bands. In this limit, g_Ω can be expressed as[31]

TABLE V. Comparison of experimental and calculated $E2/M1$ mixing ratios.

		Negative-parity band							
I_i	Expt.	Theory							
		prolate				oblate			
		a	b	c	d	a	b	c	d
$\frac{5}{2}^-$	−0.09(6)	−0.17	−25.2	+0.12	+1.27	+0.22	+0.39	+0.09	+2.22
$\frac{7}{2}^-$	−0.17(7)	−0.17	−24.0	+0.11	+1.21	+0.22	+0.39	+0.08	+2.12
$\frac{9}{2}^-$	−0.13(6)	−0.15	−22.2	+0.10	+1.12	+0.20	+0.34	+0.07	+1.96
$\frac{11}{2}^-$	−0.24(6)	−0.15	−22.3	+0.10	+1.13	+0.20	+0.34	+0.08	+1.97
$\frac{13}{2}^-$	−0.07(7)	−0.14	−20.2	+0.09	+1.02	+0.18	+0.31	+0.07	+1.78
$\frac{15}{2}^-$	−0.15(5)	−0.15	−21.2	+0.10	+1.07	+0.20	+0.32	+0.07	+1.87

		Positive-parity band			
I_i	Expt[e]	Theory			
		Prolate		Oblate	
		f	g	f	g
$\frac{7}{2}^+$	−0.22(8)	−0.16	+0.64	+0.17	+0.36
$\frac{9}{2}^+$	−0.26(6)	−0.14	+0.55	+0.14	+0.31
$\frac{11}{2}^+$	−0.37(16)	−0.27	+1.09	+0.28	+0.61
$\frac{13}{2}^+$	$-0.18(^{10}_{8})$	−0.15	+0.59	+0.15	+0.33

[a] $[301]\frac{3}{2}^-$.
[b] $[303]\frac{5}{2}^-$.
[c] $[301]\frac{1}{2}^-$, not corrected for decoupling parameter.
[d] $[312]\frac{3}{2}^-$.
[e] Taken from Reference 20.
[f] $[422]\frac{5}{2}^+$.
[g] $[431]\frac{1}{2}^+$, not corrected for decoupling parameter.

$$g_\Omega = g_l + [(g_s - g_l)/2\Omega] \sum (|a_{l,+1/2}|^2 - |a_{l,-1/2}|^2) , \quad (2)$$

where $a_{l,\pm 1/2}$ are the coefficients of the Nilsson wave functions in a spherical basis. In the calculations, we used $g_R \approx Z/A = 0.48$, $g_s = 0.7 g_s^{\text{free}}$, and the $a_{l,\pm 1/2}$ coefficients given in Ref. 32 for prolate and oblate deformations $\beta_2 = 0.42$ corresponding to $|Q_t| = 3.5$ b. The decoupling term in (1) was neglected in the $\Omega = \frac{1}{2}$ orbits due to the small signature splittings observed.

The calculated mixing ratios for different Nilsson orbits are compared in Table V with the experimental values. For the negative-parity states, the $[301]\frac{3}{2}^-$ assignment is confirmed and a *prolate* deformation can be unambiguously concluded, since there is no evidence for a triaxial shape in this band, which would lead to Ω mixing (see Sec. IV B). The situation is more complicated in the positive-parity band: As the predicted energies of the $[301]\frac{3}{2}^-$ and $[431]\frac{1}{2}^+$ single-particle states are equal at $\beta_2 \approx 0.4$ (Ref. 8), one would rather expect the $[431]\frac{1}{2}^+$ state to be lower in energy. Indeed, a regular $\Delta I = 1$ rotational band in ^{81}Sr based on this orbit, with no signature splitting and $\beta_2 \approx 0.4$, has recently been identified by Moore *et al.*[7] In ^{77}Kr a partially decoupled band with $\beta_2 \approx 0.34$, based on the $[422]\frac{5}{2}^+$ orbit, was observed by Nolte *et al.*[33] and Wörmann *et al.*[9] In ^{79}Sr, the sign and magnitude of the mixing ratios uniquely determine the $[422]\frac{5}{2}^+$ orbit as the yrast structure, again with prolate shape.

B. Deformation parameters

The experimental $E2$ and $M1$ transition strengths and quadrupole moments calculated from the $B(E2)$ values for the $\Omega = \frac{3}{2}$ (negative-parity) and the $\Omega = \frac{5}{2}$ (positive-parity) orbits are given in Table VI and are further illustrated in Fig. 7. In the positive-parity band, the $|Q_t|$

TABLE VI. $B(E2)$ and $B(M1)$ values and transitional quadrupole moments in ^{79}Sr.

E_x (keV)	I_i^π	I_f^π	δ[a]	$B(M1)$ ($\mu_N{}^2$)	$B(E2)$ ($e^2\text{fm}^4$)	$\lvert Q_t\rvert$ (b)
159	$\frac{5}{2}^-$	$\frac{3}{2}^-$	−0.09(6)	0.20(3)	$780(^{1730}_{700})$	$1.5(^{12}_{10})$
381	$\frac{7}{2}^-$	$\frac{3}{2}^-$	$E2$		$860(^{230}_{170})$	$2.46(^{31}_{26})$
		$\frac{5}{2}^-$	−0.17(7)	$0.24(^{6}_{4})$	$1990(^{3650}_{1410})$	$3.1(^{20}_{14})$
649	$\frac{9}{2}^-$	$\frac{5}{2}^-$	$E2$		$2690(^{680}_{490})$	$3.55(^{43}_{24})$
		$\frac{7}{2}^-$	−0.13(6)	$0.40(^{11}_{7})$	$1330(^{2130}_{1000})$	$3.1(^{19}_{16})$
982	$\frac{11}{2}^-$	$\frac{7}{2}^-$	$E2$		$3610(^{960}_{730})$	$3.78(^{47}_{41})$
		$\frac{9}{2}^-$	−0.24(6)	$0.47(^{14}_{11})$	$3450(^{3300}_{1880})$	$6.0(^{23}_{20})$
1339	$\frac{13}{2}^-$	$\frac{9}{2}^-$	$E2$		$2840(^{690}_{500})$	$3.19(^{37}_{29})$
		$\frac{11}{2}^-$	−0.07(7)	$0.32(^{10}_{8})$	$180(^{710}_{180})$	$1.6(^{15}_{16})$
1773	$\frac{15}{2}^-$	$\frac{11}{2}^-$	$E2$		≥ 1320	≥ 2.1
		$\frac{13}{2}^-$	−0.15(5)	> 0.08	≥ 70	≥ 1.1
2201	$\frac{17}{2}^-$	$\frac{13}{2}^-$	$E2$		$1460(^{390}_{270})$	$2.18(^{27}_{21})$
		$\frac{15}{2}^-$	$\lvert\delta\rvert \leq 0.5$	0.19(8)		
3214	$\frac{21}{2}^-$	$\frac{17}{2}^-$	$E2$		> 1150	> 1.9
330	$\frac{7}{2}^+$	$\frac{5}{2}^+$	−0.22(8)	0.10(1)	$2410(^{2150}_{1470})$	2.6(10)
499	$\frac{9}{2}^+$	$\frac{5}{2}^+$	$E2$		$1020(^{210}_{160})$	$3.21(^{30}_{27})$
		$\frac{7}{2}^+$	−0.26(6)	$0.20(^{4}_{3})$	$5980(^{4100}_{2780})$	4.5(12)
914	$\frac{11}{2}^+$	$\frac{7}{2}^+$	$E2$		$1850(^{340}_{280})$	$3.31(^{29}_{26})$
		$\frac{9}{2}^+$	−0.37(16)	0.17(4)	$1840(^{2200}_{1360})$	$2.8(^{13}_{14})$
1179	$\frac{13}{2}^+$	$\frac{9}{2}^+$	$E2$		$2610(^{640}_{450})$	$3.48(^{41}_{31})$
		$\frac{11}{2}^+$	$-0.18(^{10}_{8})$	$0.37(^{13}_{10})$	$2320(^{4870}_{1730})$	$3.6(^{27}_{18})$
1729	$\frac{15}{2}^+$	$\frac{11}{2}^+$	$E2$		≥ 1430	≥ 2.4
2064	$\frac{17}{2}^+$	$\frac{13}{2}^+$	$E2$		$1920(^{380}_{210})$	$2.68(^{25}_{15})$
		$\frac{15}{2}^+$	$\lvert\delta\rvert \leq 1$	0.18(8)		
3214	$\frac{21}{2}^+$	$\frac{17}{2}^+$	$E2$		$940(^{270}_{180})$	$1.78(^{24}_{18})$
4303	$\frac{25}{2}^+$	$\frac{21}{2}^+$	$E2$		≥ 1220	≥ 2.0

[a]From References 1 and 20.

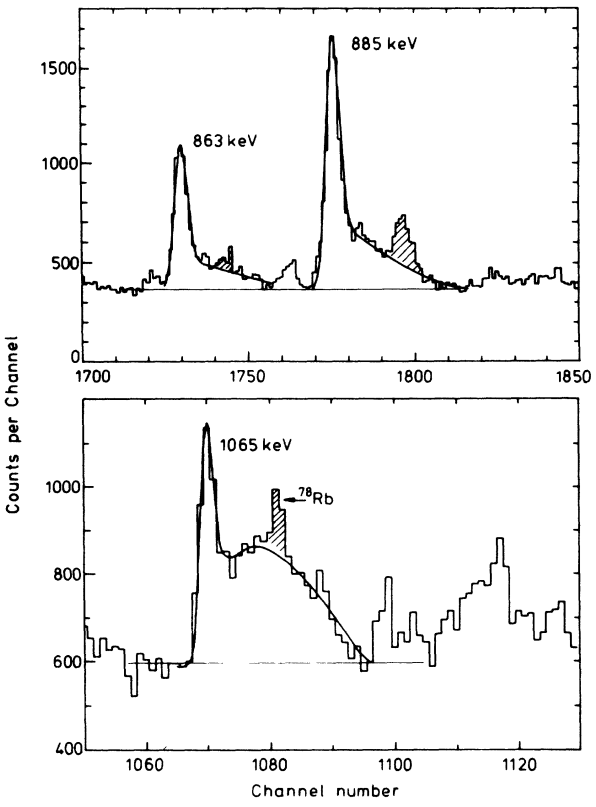

FIG. 6. Doppler broadened line shapes of several ^{79}Sr transitions. The hatched lines are contaminants not considered in the fits which are inserted as full lines.

values are constant up to $\hbar\omega \approx 0.4$ MeV; their average value $|Q_t| = 3.3(3)$ b corresponds to $\beta_2 = 0.40(4)$ in the limit of a rigid spheroid with radius $R_0 = 1.2\ A^{1/3}$ fm. The negative-parity band shows a slightly reduced $\frac{7}{2} \rightarrow \frac{3}{2}^-$ transition strength, but the quadrupole moments of the $\frac{9}{2}^-$, $1\frac{1}{2}^-$, and $\frac{13}{2}^-$ states are again in agreement and average to $|Q_t| = 3.5(3)$ b or $\beta_2 = 0.44(4)$. In both bands, reductions of $|Q_t|$ and β_2 take place at $\hbar\omega \approx 0.45$ MeV, i.e., at the onset of the first band crossings (see Sec. IV C). It appears that this (most probable $g_{9/2}$ proton) alignment causes a decrease in collectivity of about 40% in both bands.

So far we have assumed axial symmetry in the analysis, while there is ample evidence for nonaxial nuclear shapes in many odd-Z nuclei of this mass region.[13,34,35] In recent papers, Hamamoto[36] has discussed criteria for detecting nonaxial shapes in odd-A nuclei in tests in γ-ray spectroscopy. Deviations from axial symmetry are evident as (i) a signature dependence of the $B(E2, I \rightarrow I-1)$ values, (ii) an anomalous signature dependence of the $B(M1)$ values, and (iii) a signature inversion of the high-j Routhians. Criteria (i) and (ii) require precise experimental $\Delta I = 1$ $M1$ and $E2$ transition strengths to be tested. As shown in Fig. 7(b), the Q_t values obtained from the $\Delta I = -1$, $B(E2)$ values suffer from the relatively large experimental errors of the mixing ratios. Nonetheless, nearly all $|Q_t|$ values are in good agreement with the average figures deduced from the $\Delta I = 2$ transitions [see Fig. 7(a)]. In the positive-parity band, the slight signature dependence of the $Q(I \rightarrow I-1)$ would correspond to a small positive γ value.

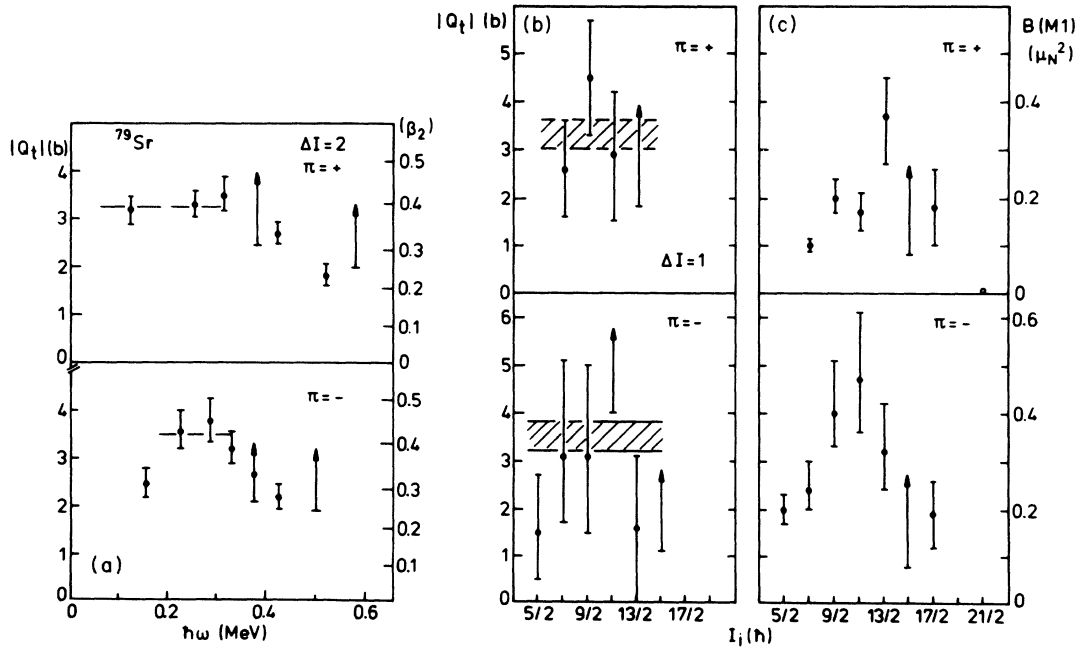

FIG. 7. (a) Experimental transitional quadrupole moments as a function of the rotational frequency for the positive- and negative-parity stretched $E2$ transitions (b) transitional quadrupole moments of $\Delta I = -1$ transitions as a function of the initial spin I_i, (c) $B(M1)$ values of $\Delta I = -1$ transitions as function of the initial spin I_i.

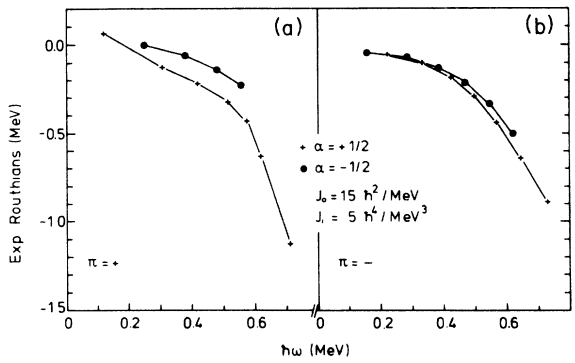

FIG. 8. Experimental neutron Routhians for the (a) positive- and (b) negative-parity yrast bands in ^{79}Sr. The Harris parameters J_0 and J_1 are inserted.

Another useful relationship to test triaxiality was proposed as[36]

$$\Delta B(M1,I_f) \equiv \{B[M1,I_f \rightarrow (I-1)] - B[M1,(I-1)_u \rightarrow (I-2)_f]\}/B(M1)_{\rm av} = 4\hbar\omega e/[(\hbar\omega)^2+(\Delta e)^2] \ . \quad (3)$$

This equation only holds in the limit of axial symmetry. Here, the indices f and u denote favored ($\alpha=+\frac{1}{2}$) and unfavored signatures ($\alpha=-\frac{1}{2}$), respectively, Δe is the energy difference between the $\alpha=\pm\frac{1}{2}$ Routhians, and $B(M1)_{\rm av}$ is the average $B(M1)$ transition strength

$$B(M1)_{\rm av} \equiv \tfrac{1}{2}\{B[M1,I_f \rightarrow (I-1)_u] + B[M1,(I-1)_u \rightarrow (I-2)_f]\} \ . \quad (4)$$

The experimental Routhians of the positive- and negative-parity yrast bands are plotted in Fig. 8. In the negative-parity band very little signature splitting is visible ($\Delta e \approx 0$) and the $B(M1)$ values of subsequent transitions overlap within their errors bars so as to fulfill Eq. (3). The positive-parity band shows a small signature splitting of $\Delta e = 90-130$ keV, but no signature inversion of the favored and unfavored Routhians. The left- and right-hand side of Eq. (3) can be calculated for the sequences $\frac{13}{2}^+ \rightarrow \frac{11}{2}^+ \rightarrow \frac{9}{2}^+$ and $\frac{9}{2}^+ \rightarrow \frac{7}{2}^+ \rightarrow \frac{5}{2}^+$, giving $\Delta B(M1,\frac{13}{2}) = 0.7(5)$ and $\Delta B(M1,\frac{9}{2}) = 2.0(8)$ for the left-hand side to be compared with 1.2 and 2.0 for the right-hand side of Eq. (3). Thus we may safely conclude that the negative-parity band has axial symmetry up to spin $\frac{15}{2}^-$. For the positive-parity band, we cannot fully exclude a triaxial shape, but as all requirements for axial symmetry are fulfilled, it seems unlikely that the odd $g_{9/2}$ neutron induces a large asymmetry of the core. None the less, more precise δ values are desirable in order to pursue this question.

C. Alignment properties

Figure 9(a) illustrates the dynamical moment of inertia $J^{(2)}$ in the $\alpha=\pm\frac{1}{2}$ negative-parity bands in comparison with the ground band in ^{78}Sr (Ref. 37). All three bands show broad peaks of $J^{(2)}$ at $\hbar\omega = 0.4-0.6$ MeV, indicating strong band mixings. Following the arguments given in Refs. 2 and 37, this mixing most probably arises from $g_{9/2}$ proton ($2qp$) alignment. The aligned quasiparticle alignment in the $\pi=-1$ bands in ^{79}Sr amounts to $i=2.8\hbar$.

The most obvious irregularity in the observed level sequence is the pronounced upbend in the positive-parity

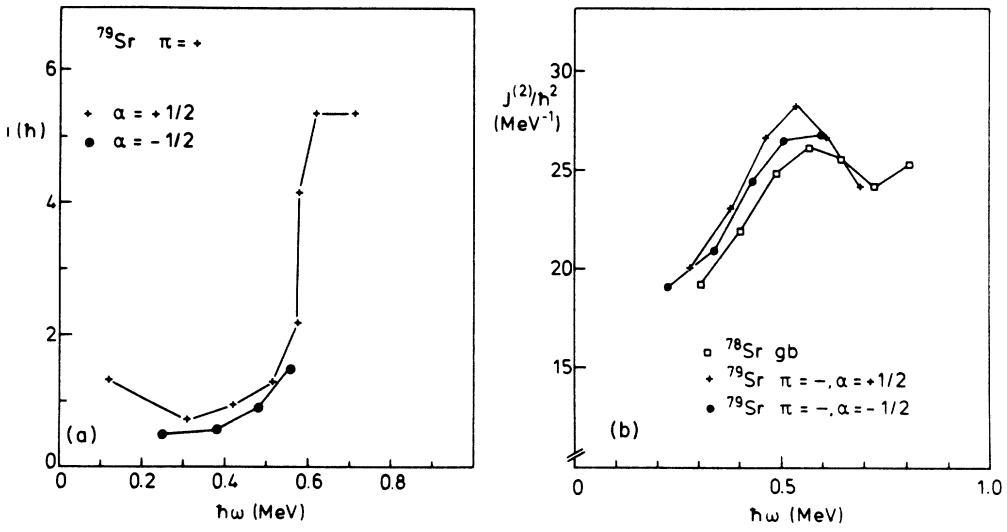

FIG. 9. (a) The plot of the aligned single-particle momentum for the ^{79}Sr positive-parity bands. The Harris parameters used to obtain this curve are $J_0 = 15\ \hbar^2/\text{MeV}$ and $J_2 = 5\ \hbar^4/\text{MeV}^3$. (b) The dynamic moment of inertia J^2 for the ^{79}Sr negative-parity bands compared with the ground-state band of ^{78}Sr.

band observed by Chishti *et al.*[11] which clearly is in contrast to the gradual alignment found for the negative-parity states. In Fig. 9(a) the aligned quasiparticle angular momentum i in this band is plotted versus $\hbar\omega$; i increases gradually by $0.7\hbar$ in the range $\hbar\omega \approx 0.3-0.52$ MeV and rapidly increases by another $3.7\hbar$ during the upbend at $\hbar\omega = 0.58$ MeV. The total gain in quasiparticle spin amounts to $4.4\hbar$. The shape of this $i(\omega)$ curve seems

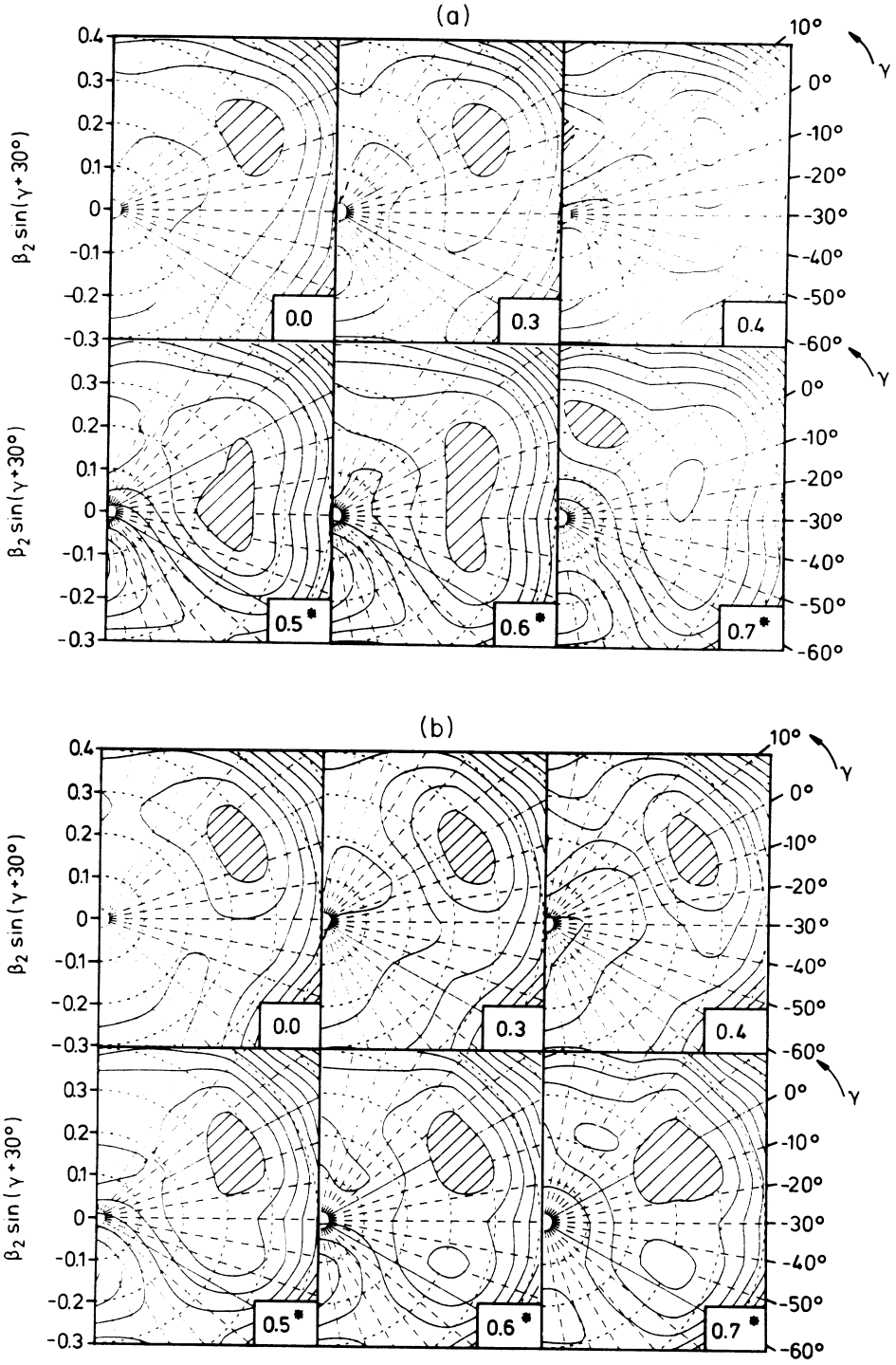

FIG. 10. Shape evolution as a function of the rotational frequency for the ^{79}Sr (a) positive-parity and (b) negative-parity favored bands. The insets show the rotational frequency in MeV, asterisks denote TRS calculated for $(2qp)_\pi(1qp)_\nu$ configurations. The hatched areas correspond to excitation energies ≤ 0.4 MeV above the minimum, the energy difference between the contour lines is 0.8 MeV.

to be quite puzzling. If the upbend was due to a $g_{9/2}$ ($2pq$) neutron crossing, one should see a similar crossing in the negative-parity band (where $g_{9/2}$ neutron alignment is not blocked), unless there is a drastic shape change between the positive- and negative-parity ($3qp$) bands. Such second-band crossing has not been found. Of course, one may also consider a more complicated scenario recently suggested for the positive-parity yrast band of ^{76}Kr:[38] here the $g_{9/2}$ proton and neutron alignments are found to coincide at $\hbar\omega=0.65$ MeV. The aligned protons seem to reduce the deformation in such a way that the neutron alignment frequency is lowered. A similar effect may also be present in the positive-parity band of ^{79}Sr, as indicated by the strongly reduced deformation on the basis of $B(E2)$ values [see Fig. 7(a)].

D. Woods-Saxon cranking calculations

The influence of collective rotation and particle alignments on the shape of ^{79}Sr has also been considered from the point of view of the Strutinsky-Bogolubov cranking model with a deformed Woods-Saxon potential.[8] Details of the model and the input parameters in the $A=80$ region are given in recent work of Nazarewicz[39] and Gross *et al.*[40] As a first step, the total Routhian surfaces (TRS) in ^{79}Sr were calculated for the ($1qp_n$) neutron configurations. The shape evolution in ^{79}Sr as a function of the rotational frequency is shown in Figs. 10(a) and 10(b) for the positive- and negative-parity favored bands, respectively. The hatched areas correspond to an energy of less than 0.4 MeV above the minimum, the energy difference between the contour lines is 0.8 MeV. At small rotational frequencies ($\hbar\omega\leq 0.4$ MeV) a stable minimum is predicted at deformations $\beta_2\approx 0.37$, $\gamma\approx 0°$. This value is in good agreement with the experiment if one considers that the experimental charge deformation has to be reduced by 10% to yield the Woods-Saxon deformation parameter.[41] At those deformations, the $g_{9/2}$ proton ($2qp$) alignment is expected to take place at $\hbar\omega=0.4$–0.5 MeV with a large interaction as shown in Fig. 11(a).

The neutron crossing is shifted up to a much higher angular frequency of $\hbar\omega\approx 1$ MeV. The TRS for rotational frequencies $\hbar\omega\geq 0.5$ MeV have thus been calculated for the $(2qp)_\pi(1qp)_\nu$ configurations and are labeled with asterisks in Figs. 10 (a) and (b). The $3qp$ TRS for the positive-parity $\alpha=+\frac{1}{2}$ band show a decrease in quadrupole deformation and less defined γ values, while in the negative-parity TRS minimum stays at $\beta_2\approx 0.37$, $\gamma\approx 0°$. This is in agreement with the observed alignment properties in the negative-parity band associated with $g_{9/2}$ protons. On the other hand, it can be seen in Fig. 10 that the proton crossing induces a strong shape change in the positive parity band. The upbend in this band can be explained by angular momentum alignments of $g_{9/2}$ protons causing a transition to negative γ values. In fact such a tendency has already been predicted for ^{80}Sr (Ref. 8). Neutron quasiparticle Routhians calculated for deformations corresponding to the minimum in the $3qp$ TRS, i.e., $\beta_2=0.26, \gamma=-30°$, are displayed in Fig. 12. At this deformation, the BC crossing has a large interaction leading to a very smooth angular momentum alignment at $h\omega>0.6$ MeV. At the moment, no experimental data are

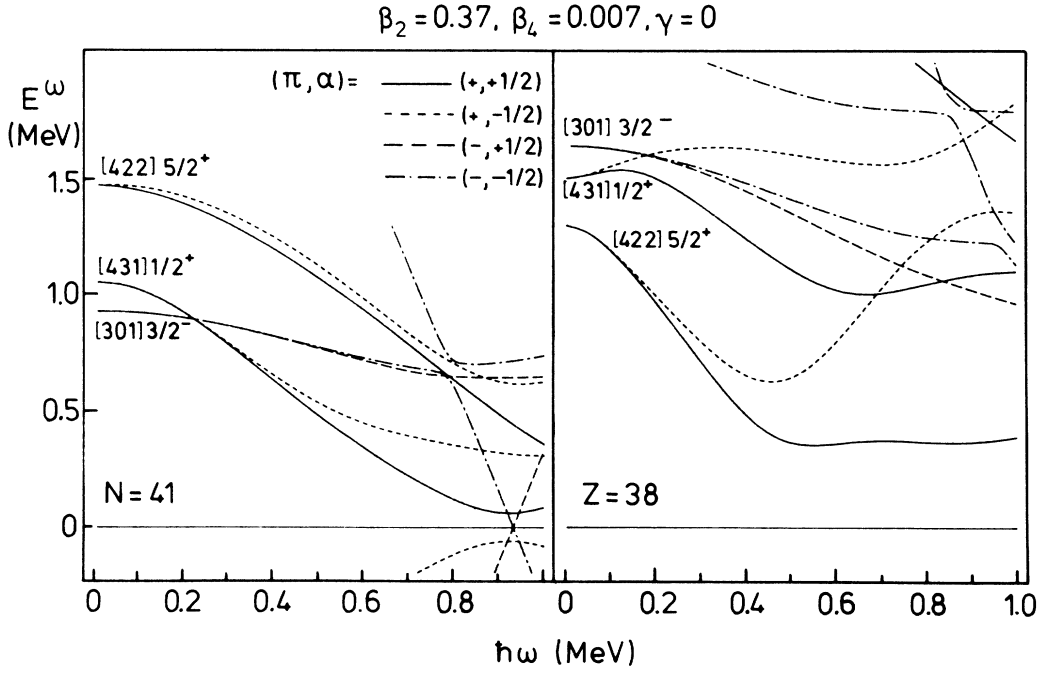

FIG. 11. Proton and neutron Woods-Saxon quasiparticle Routhians for ^{79}Sr at a deformation $\beta_2=0.37$, $\beta_4=-0.007$, and $\gamma=0°$.

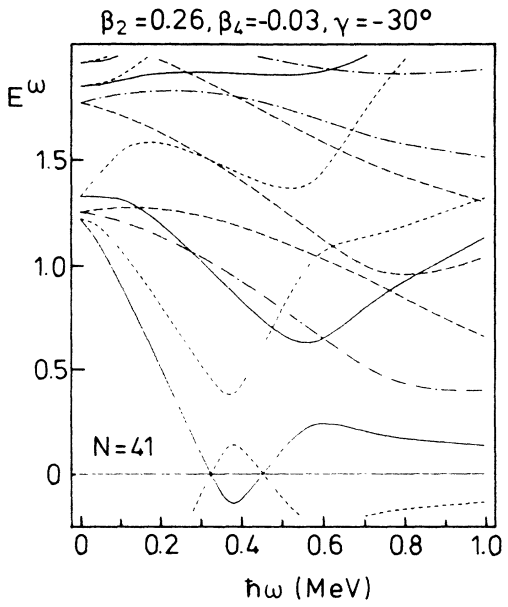

FIG. 12. Neutron quasiparticle Routhians at deformations $\beta_2=0.26$, $\beta_4=-0.03$, and $\gamma=-30°$.

available at these high rotational frequencies to test this prediction.

V. CONCLUSIONS

In the present work, lifetimes have been determined in the positive- and negative-parity yrast bands in ^{79}Sr extending into the $(1qp)\rightarrow(3qp)$ band crossing region. A systematic comparison of lifetimes in ^{79,70,82}Sr obtained from recoil distance and DSA experiments indicated that the Ziegler-Biersack-Littmark parametrization of the electronic stopping power well describes the slowing down of fast Sr ions in Ta.

By making use of the measured $E2/M1$ mixing ratios, the positive- and negative-parity $(1qp)$ bands have been found to be based on the $[422]\frac{5}{2}^+$ and $[301]\frac{3}{2}^-$ Nilsson orbits, at large *prolate* deformations of $\beta_2^+=0.40(4)$ and $\beta_2^-=0.44(4)$, respectively. In the $[422]\frac{5}{2}^+$ orbit, the neutron does not induce a core polarization towards larger deformation. In this respect, the situation is very similar to the one found in the isotone ^{77}Kr (Refs. 9 and 42). In the $(1qp)$ bands no evidence for strong triaxiality has been found below spin $\frac{15}{2}$, either from the signature splitting or the staggering of $M1$ and $E2$ transition strengths. Cranked shell-model and Hartree-Fock-Bogolyubov calculations support this interpretation.

In the transition region to $(3qp)$ alignment, the quadrupole moments in both bands show a very similar behavior; they decrease by about 40% at $\hbar\omega\approx0.45$ MeV. This drop in collectivity is probably associated with the alignment of a $g_{9/2}$ proton pairs, as suggested by Hartree-Fock-Bogolyubov cranking calculations.

ACKNOWLEDGMENTS

The authors would like to thank the crew of the tandem accelerator at Oxford University for providing excellent ^{24}Mg beams and their encouragement. The help of W. Fieber, C. J. Gross, J. Eberth, and S. Skoda during the ^{32}S+^{54}Fe experiment is very much appreciated. We would also like to thank K. Bharuth-Ram for his help in the ^{80}Sr recoil distance lifetime analysis and to W. Nazarewicz for the permission to quote unpublished results. This research has been partially funded by Deutsches Bundesministerium für Forschung und Technologie (Contract No. 06 Gö 141) and by grants from the United Kingdom Science and Engineering Research Council.

*Present address: The United Kingdom Science and Engineering Research Council, Daresbury Laboratory, Warrington WA4 4AD, United Kingdom.

†Present address: A. W. Wright Nuclear Structure Laboratory, Yale University, New Haven, CT 06511.

[1]C. J. Lister, B. J. Varley, H. G. Price, and J. W. Olness, Phys. Rev. Lett. **48**, 308 (1982).

[2]R. F. Davie, D. Sinclair, S. Ooi, N. Poffe, A. Smith, H. G. Price, C. J. Lister, B. J. Varley, and I. F. Wright, Nucl. Phys. **A463**, 683 (1987).

[3]P. S. Haskins, F. E. Dunham, R. L. Caldwell, A. C. Rester, R. B. Piercey, M. L. Muga, H. A. van Rinsvelt, R. W. Smart, H. J. M. Aarts, J. D. Fox, L. C. Dennis, and C. B. Saw, Phys. Rev. C **32**, 1897 (1985).

[4]A. Dewald, U. Kaup, W. Gast, A. Gelberg, H.-W. Schuh, K. O. Zell, and P. von Brentano, Phys. Rev. C **13**, 1217 (1976).

[5]C. Broude, E. Dafni, A. Gelberg, M. B. Goldberg, G. Goldring, M. Hass, O. C. Kistner, and A. Zemel, Phys. Lett. **105B**, 119 (1981).

[6]A. I. Kucharska, J. Billowes, and C. J. Lister, in *Nuclear Structure in the Zirconium Region*, edited by J. Eberth, R. A. Meyer, and K. Sistemich (Springer, Berlin, 1988), p. 161.

[7]E. F. Moore, P. D. Cottle, C. J. Gross, D. M. Headly, U. J. Hüttmeier, S. L. Tabor, and W. Nazarewicz, Phys. Rev. C **38**, 696 (1988); Phys. Lett. B **211**, 14 (1988).

[8]W. Nazarewicz, J. Dudek, R. Bengtsson, T. Bengtsson, and I. Ragnarsson, Nucl. Phys. **A435**, 397 (1985).

[9]B. Wörmann, K. P. Lieb, R. Diller, L. Lühmann, J. Keinonen, L. Cleemann, and J. Eberth, Nucl. Phys. **A431**, 170 (1984).

[10]L. Funke, J. Döring, P. Kemnitz, E. Will, G. Winter, A. Johnson, L. Hildingsson, and Th. Lindblad, Phys. Rev. C **25**, 226 (1982); Nucl. Phys. **A455**, 206 (1986).

[11]A. A. Chishti, M. Campbell, W. Gelletly, L. Goettig, A. N. James, C. J. Lister, D. J. G. Love, J. H. McNeill, R. Moscrop, O. Skeppstedt, and B. J. Varley, *Nuclear Structure of the Zirconium Region*, edited by J. Eberth, R. A. Meyer, and K. Sistemich (Springer, Berlin, 1988), p. 320.

[12]K. P. Lieb, M. Uhrmacher, J. Dauk, and A. M. Kleinfeld,

Nucl. Phys. **A223**, 445 (1974).
[13]J. Panqueva, H. P. Hellmeister, L. Lühmann, F. J. Bergmeister, K. P. Lieb, and T. Otsuka, Nucl. Phys. **A389**, 424 (1982).
[14]H. P. Hellmeister and L. Lühmann, computer code CHRONOS, Göttingen, 1981 (unpublished).
[15]R. Rascher, K. P. Lieb, and M. Uhrmacher, Phys. Rev. C **13**, 1217 (1976).
[16]W. Gelletly, Y. Abdelrahman, A. A. Chishti, J. L. Durell, J. Fitzgerald, C. J. Lister, J. H. McNeil, W. R. Phillips, and B. J. Varley, in *Nuclear Structure of the Zirconium Region,* edited by J. Eberth, R. A. Meyer, and K. Sistemich (Springer, Berlin, 1988), p. 101.
[17]H. P. Hellmeister and L. Lümann, computer code GNOMON, Göttingen, 1983 (unpublished).
[18]F. Cristancho, J. Heese, K. P. Lieb, C. J. Gross, W. Fieber, Th. Osipowicz, S. Ulbig, S. Skoda, J. Eberth, A. Dewald, and P. von Brentano, Nucl. Phys. **A501**, 118 (1989).
[19]W. Fieber, K. Bharuth-Ram, J. Heese, F. Cristancho, C. J. Gross, K. P. Lieb, S. Skoda, and J. Eberth, Z. Phys. A **332**, 363 (1989).
[20]C. J. Lister and A. A. Chishti (private communication).
[21]F. Cristancho and K. P. Lieb, Nucl. Phys. **A456**, 353 (1988).
[22]L. Lühmann, M. Debray, K. P. Lieb, W. Nazarewicz, B. Wörmann, J. Eberth, and T. Heck, Phys. Rev. C **31**, 828 (1985).
[23]J. Heese, K. P. Lieb, L. Lühmann, F. Raether, B. Wörmann, D. Alber, H. Grawe, J. Eberth, and T. Mylaeus, Z. Phys. A **325**, 45 (1986).
[24]J. Heese, K. P. Lieb, L. Lühmann, S. Ulbig, B. Wörmann, D. Alber, H. Grawe, H. Haas, and B. Spellmeyer, Phys. Rev. C **36**, 2409 (1987).
[25]A. Dewald, U. Kaup, W. Gast, A. Gelberg, K. O. Zell, and P. V. Brentano, Proceedings of the International Conference on Nuclei Far from Stability, Helsingor, 1981, CERN Report No. CERN-81-09, 1981, p. 418.
[26]S. Kalbitzer and H. Oetzmann, Proceedings of the International Conference of Materials, Budapest, 1978 (unpublished).
[27]A. E. Blaugrund, Nucl. Phys. **88**, 501 (1966).
[28]L. C. Northcliffe and R. F. Schilling, Nucl. Data Tables **A9**, 233 (1970).
[29]J. F. Ziegeler, J. P. Biersack, and U. Littmark, *The Stopping and Range of Ions in Solids* (pergamon, New York, 1985).
[30]F. Buchinger, E. B. Ramsay, R. E. Silverans, P. Lievens, E. Arnold, W. Neu, R. Neugart, K. Wendt, and G. Ulm, Z. Phys. A **327**, 361 (1987).
[31]H. Morinaga and T. Yamazaki, *In-Beam Gamma-Ray Spectroscopy* (North-Holland, Amsterdam, 1976).
[32]S. G. Nilsson, Dan. Mat. Fys. Medd. **29**, No. 16 (1955).
[33]E. Nolte and P. Vogt, Z. Phys. A **275**, 33 (1975).
[34]L. Lühmann, K. P. Lieb, C. J. Lister, J. W. Olness, H. G. Price, and B. J. Varley, Europhys. Lett. **1**, 623 (1986).
[35]K. P. Lieb, L. Lühmann, and B. Wörmann, in *Nuclei Off the Line of Stability,* edited by R. A. Meyer and D. S. Brenner (American Chemical Society, Washington, D.C., 1986), p. 233.
[36]I. Hamamoto, 4th Franco-Japanese Colloquim, Seillac, 1986, [Report Lund-Mph-86/15 (unpublished)].
[37]C. J. Gross, J. Heese, K. P. Lieb, C. J. Lister, B. J. Varley, A. A. Chishti, J. H. McNeill, and W. Gelletly, Phys. Rev. C **39**, 1780 (1989).
[38]C. J. Gross, J. Heese, K. P. Lieb, S. Ulbig, W. Nazareqicz, C. J. Lister, B. J. Varley, J. Billowes, A. A. Chishty, J. H. McNeill, and W. Gelletly, Nucl. Phys. **A501**, 367 (1989).
[39]W. Nazarewicz (private communication).
[40]C. J. Gross, P. D. Cottle, D. M. Headly, U. J. Hüttmeier, E. F. Moore, S. L. Tabor, and W. Nazarewicz, Phys. Rev. C **36**, 2601 (1987).
[41]J. Dudek, W. Nazarewicz, and P. Olanders, Nucl. Phys. **A420**, 285 (1984).
[42]E. Nolte, Y. Shida, W. Kutschera, R. Prestele, and H. Morinaga, Z. Phys. **268**, 267 (1974).